membranes

MDPI

Article

Performance Evaluation of a Membrane-Based Desorber Operating with the LiBr + LiCl/H_2O Mixture for Intermittent Absorption Systems

Jonathan Ibarra-Bahena [1], Ulises Dehesa-Carrasco [2,3], Yuridiana Rocio Galindo-Luna [4], Arelis Ledesma-Juárez [1] and Wilfrido Rivera [1,*]

[1] Instituto de Energías Renovables, Universidad Nacional Autónoma de México, Privada Xochicalco S/N, Temixco 62580, Morelos, Mexico; jibarra@ier.unam.mx (J.I.-B.); arelis@ier.unam.mx (A.L.-J.)
[2] Instituto de Ingeniería, Universidad Nacional Autónoma de México, Cd. Universitaria, Coyoacán, Ciudad de México 04510, Mexico; udehesac@iingen.unam.mx
[3] El Colegio de Chihuahua, Partido Díaz 4723, Cd. Juárez 32310, Chihuahua, Mexico
[4] Departamento de Ingeniería de Procesos e Hidráulica, Universidad Autónoma Metropolitana-Iztapalapa. Av. Ferrocarril San Rafael Atlixco 186, Col. Leyes de Reforma 1 A Sección, Iztapalapa, Ciudad de México 09310, Mexico; ygalindol@izt.uam.mx
* Correspondence: wrgf@ier.unam.mx

Abstract

Absorption cooling systems can operate using thermal energy supplied by renewable sources or recovered from low-grade waste heat, providing an alternative to vapor-compression cooling technologies. Intermittent operation is particularly suitable for applications with variable heat availability because it decouples the desorption and absorption processes, requiring desorption devices capable of stable operation. In this work, a membrane-based desorber operating with a LiBr + LiCl/H_2O mixture (mass ratio 2:1, LiBr:LiCl) was experimentally evaluated for intermittent absorption cooling system applications. Two polytetrafluoroethylene (PTFE) membranes with pore sizes of 0.22 and 0.45 μm and two initial salt concentrations of 50.01 ± 0.06% and 44.96 ± 0.01% *w*/*w* were tested at solution and cooling-water temperatures of 90.2 ± 0.1 °C and 30.0 ± 0.1 °C, respectively. After 3 h of operation, cumulative distilled water production ranged from 5.36 ± 0.17 to 11.03 ± 0.10 kg/m^2, with the highest production corresponding to the 0.45 μm membrane and an initial salt concentration of 44.96% *w*/*w*. Under the comparable operating conditions evaluated, LiBr/H_2O produced 69.9% more cumulative distilled water than LiBr + LiCl/H_2O, while LiBr + LiCl/H_2O produced 22.4% more than LiCl/H_2O. However, at an initial salt concentration of 44.96% *w*/*w* and using a 0.22 μm membrane, LiBr + LiCl/H_2O produced only 1.8% less cumulative distilled water than LiBr/H_2O at 49.59% w/w using a 0.45 μm membrane. When a 0.45 μm membrane was used for both solutions, LiBr + LiCl/H_2O produced 15.4% more cumulative distilled water than LiBr/H_2O. These results indicate the potential of LiBr + LiCl/H_2O as a competitive alternative to conventional mixtures used in intermittent absorption cooling systems.

Keywords: air gap membrane distillation; intermittent absorption cooling systems; LiBr + LiCl/H_2O mixture

Academic Editor: Francesca Macedonio

Received: 4 October 2026
Revised: 21 October 2026
Accepted: 25 November 2026
Published: 27 November 2026

Copyright: © 2026 by the authors. Licensee MDPI, Basel, Switzerland. This article is an open access article distributed under the terms and conditions of the Creative Commons Attribution (CC BY) license.

1. Introduction

Decarbonizing the energy sector demands technologies that can operate with low-grade heat, especially as global warming increases cooling and air-conditioning requirements. According to the International Energy Agency, worldwide electricity consumption for space cooling has increased by approximately 50% since 2015, reaching nearly 2900 TWh, representing about 14% of total electricity demand growth [1]. Compared with conventional vapor-compression refrigeration systems, absorption cooling systems can operate using thermal energy instead of mechanical compression, allowing the use of low-grade heat sources, including solar thermal energy and industrial waste heat. Consequently, these systems can reduce electricity consumption, particularly when renewable energy or waste heat is available [2,3].

Absorption cooling systems operate through a thermally driven refrigeration cycle that includes four main components: an evaporator, an absorber, a desorber (generator), and a condenser. In the evaporator, the refrigerant absorbs heat from the medium to be cooled as it evaporates at low pressure. The resulting vapor is absorbed by the absorbent solution, releasing heat that must be removed to maintain the absorption process. The diluted solution is then pumped to the generator, where thermal energy is supplied to separate the refrigerant from the absorbent. The refrigerant vapor is subsequently condensed, while the concentrated solution returns to the absorber. The condensed refrigerant is returned to the evaporator through an expansion device [4].

Among the different absorption cooling system configurations, intermittent operation separates the desorption (also known as generation) and absorption processes into two separate stages. During desorption, thermal energy is supplied to the absorbent solution to separate the refrigerant, which is subsequently condensed and stored for later use. This configuration allows the refrigerant produced during the regeneration stage to be used for cooling at a different time, depending on cooling demand, without requiring the simultaneous operation of both stages. This configuration can reduce capital costs compared with continuous-mode systems and simplify operation and maintenance [5].

Several authors have studied this configuration: Nguyen et al. [6] analyzed an intermittent absorption refrigeration prototype that used the H_2O/NH_3 mixture to produce 2 kg of ice under Vietnam's climatic conditions. Using a thermodynamic model, the authors evaluated system performance as a function of the generation, evaporation, and ambient temperatures. The predicted Coefficient of Performance (COP) ranged between 0.19 and 0.26, with the optimum generation temperature varying from 112 to 142 °C, whereas the experimental COP ranged from 0.064 to 0.110. This discrepancy was attributed to high heat losses, progressive weakening of the absorption process, and undesired increases in solution temperature and pressure during generation, which deviated from the modeled conditions. The experimental system produced approximately 1 kg of ice per cycle. These results demonstrate the technical feasibility of operating intermittent absorption systems using thermal energy supplied within the investigated temperature range. Ibarra-Bahena et al. [7] investigated an intermittent absorption cooling configuration in which desorption and condensation were carried out using a hydrophobic membrane device operating under the Air Gap Membrane Distillation (AGMD) principle. The system used $LiBr/H_2O$ as the working mixture and solar thermal energy as the heat source. The authors experimentally evaluated the membrane unit, which produced 14.50, 11.59, and 7.20 kg/m^2 of refrigerant after 4 h at solution temperatures of 95.1, 85.2, and 75.1 °C, respectively. A larger-scale solar-driven intermittent cooling system was sized using these experimental results, requiring 20.9–30.2 m^2 of solar collector area and achieving evaporator temperatures between 12 and 18 °C. The resulting COP values were 0.15, 0.21, and 0.26, increasing with desorber temperature. Ibrahim and Dincer [8] evaluated a combined solar system designed for rural applications that simultaneously produces potable water and cooling. The

https://doi.org/10.3390/membranes16120406

proposed system integrates a solar still operating under sub-atmospheric pressure with an intermittent LiBr/H_2O absorption cooling unit powered by photovoltaic panels. The authors reported a maximum desalination unit efficiency of 40%, with an evaporator temperature of 4.7 °C. The overall energy efficiency of the system reached 13.75%. Rivera et al. [9] experimentally investigated an intermittent absorption refrigeration system using $LiNO_3/NH_3$ and solar thermal energy as the heat source. The system produced ice without requiring an external electrical energy supply, with the evaporator reaching a minimum temperature of −11 °C. Their experimental results confirmed the viability of low-cost solar-thermal absorption cycles for rural areas. Using this configuration as a baseline, Moreno-Quintanar et al. [10] evaluated a ternary $LiNO_3/NH_3/H_2O$ solution, reporting enhanced heat- and mass-transfer performance, reduced generation temperatures, and solar COP improvements of up to 24% relative to the binary mixture.

While intermittent absorption systems offer a cost-effective pathway for utilizing low-temperature renewable heat, their performance strongly depends on the thermodynamic and transport properties of the working solution. The choice of refrigerant–absorbent mixture determines key operational parameters such as generation temperature, vapor pressure, crystallization limits, and heat and mass-transfer behavior, all of which directly influence refrigerant production during the desorption step [11,12]. Mixed-salt solutions provide an opportunity to improve desorption performance in intermittent systems. In particular, the ternary LiBr + LiCl/H_2O (2:1 mass ratio) mixture offers favorable characteristics. According to Arabi and Dehghani [13], this mixture exhibits higher solubility than conventional LiBr solution, mitigating crystallization risks, and its lower density reduces pumping power, both desirable features for stable operation in intermittent absorption systems. Recent studies have reported additional advantages of this mixture in absorption systems: Aktemur and Öztürk [14] evaluated the LiBr + LiCl/H_2O mixture with a 2:1 salt mass ratio in a single-effect absorption chiller coupled to a solar thermal system. The performance of the ternary mixture was compared with that of LiBr/H_2O. Their results showed that the ternary mixture reduced the circulation ratio by 48.93% and the required collector area by 8.92%, while increasing the COP, solar COP, and exergy efficiency by 8.81%, 8.88%, and 8.96%, respectively. These results confirm that LiBr + LiCl/H_2O (2:1) enhances system efficiency and reduces solar field requirements under realistic operating conditions. In another study [15], the authors optimized generator temperature for the same ternary mixture and demonstrated that LiBr + LiCl/H_2O expands the safe operating conditions by reducing crystallization risk, enabling operation at lower generator temperatures. Additionally, Ibarra-Bahena et al. [16] demonstrated the feasibility of using LiBr + LiCl/H_2O (2:1) in an AGMD process. The experimental results showed stable operation at high salt concentrations, with distilled-water fluxes between 0.28 and 7.63 $kg \cdot h^{-1} \cdot m^{-2}$ depending on temperature and concentration.

Although a previous study [16] demonstrated the feasibility of using the LiBr + LiCl/H_2O mixture in an AGMD process, it primarily focused on the effects of operating temperatures, salt concentration, and membrane pore size on distilled water flux. However, the time-dependent desorption performance of this mixture over a defined operating period, particularly its cumulative distilled water production and the progressive increase in salt concentration, was not investigated. These parameters are particularly relevant for intermittent absorption cooling systems, where desorption and absorption occur in separate operating stages, and the refrigerant recovered during desorption is stored for subsequent cooling operation. Furthermore, experimental information on the time-dependent desorption behavior of the LiBr + LiCl/H_2O mixture compared with conventional LiBr/H_2O and LiCl/H_2O solutions remains limited. Therefore, the present study experimentally investigates an AGMD desorber operating with a LiBr + LiCl/H_2O mixture at a 2:1 mass ratio. Distilled water production and salt concentration evolution are evaluated

over a 180 min operating period for different membrane pore sizes and initial salt concentrations. The experimental results are then compared with previously reported data for $LiBr/H_2O$ and $LiCl/H_2O$ to identify differences in their time-dependent desorption performance. This work provides new experimental evidence on the desorption behavior of the $LiBr + LiCl/H_2O$ mixture and contributes to assessing its potential as a working pair for membrane-based intermittent absorption cooling systems. The integration of desorption and condensation processes into a single membrane-based device could also contribute to reducing the complexity, size, and cost of these systems.

2. Materials and Methods

Membrane distillation (MD) is a thermally driven separation process in which vapor passes through a hydrophobic porous membrane due to a vapor pressure difference [17]. The main MD configurations are [18]: direct contact membrane distillation (DCMD), where the feed solution and the cooling fluid are in direct contact with opposite sides of the membrane; sweeping gas membrane distillation (SGMD), where a gas stream transports the vapor to an external condenser; vacuum membrane distillation (VMD), where vacuum is applied on the permeate side; and air gap membrane distillation (AGMD), where an air layer separates the membrane from the condensation surface. Another configuration is permeate gap membrane distillation (PGMD), where the space between the membrane and the condensation surface is filled with liquid permeate. In AGMD, the air gap reduces conductive heat losses, although it introduces additional resistance to mass transfer. Furthermore, the AGMD configuration allows water vapor separation and condensation within a single module at atmospheric pressure, without requiring vacuum-generating equipment for the desorption process. These characteristics offer potential advantages for simplifying membrane-based intermittent absorption cooling systems [7].

In this study, the term "membrane-based desorber" refers to a device that uses a hydrophobic porous membrane to separate water vapor from an aqueous absorbent solution through a membrane distillation process. The membrane-based desorber operates under the AGMD principle, allowing water vapor separation and condensation within the same module.

2.1. Figure Generation/Data Visualization

Figure [3] was edited using the generative artificial intelligence tool ChatGPT (GPT-6, OpenAI, San Francisco, CA, USA) with a prompt requesting an improvement in the visual presentation of the original schematic provided by the authors. The edited figure was reviewed by the authors to ensure its technical accuracy and consistency with the experimental system. The authors take full responsibility for the content of the figure.

2.2. Membrane-Based Desorber Configuration

The membrane module used in this study consisted of a compact, plate-type assembly. The device was built around two rigid polymeric plates that served as structural support and defined the flow channels. Between these plates, a sequence of gaskets and a condensation surface created the three functional regions of the AGMD configuration: the heated feed solution channel, the air gap, and the cooling-water channel. The saline solution flowed through a rectangular cavity formed by one of the polymeric plates, a heat-resistant silicone gasket, and the inner face of the hydrophobic membrane. This channel measured approximately 180 mm in length, 80 mm in width, and 3 mm in thickness, providing the pathway for the heated saline solution. To prevent membrane deformation under flow, a metallic mesh was positioned directly behind it. The air gap was defined by the membrane's rear surface, the neoprene gaskets, and the condensation plate. The gap thickness was fixed at 3 mm, allowing vapor generated at the membrane surface to

migrate toward the condensation plate. This plate, made of aluminum with a thickness of 0.4 mm, was followed by a second flow channel for the cooling water stream. This channel was delimited by another silicone gasket and the outer polymeric plate, completing the three-layer arrangement required for AGMD operation. Two commercial hydrophobic polytetrafluoroethylene (PTFE) membranes (Fluoropore®, MilliporeSigma, Burlington, MA, USA) with nominal pore sizes of 0.22 μm (FGLP29325) and 0.45 μm (FHLP29325) were evaluated. The main specifications of both membranes are summarized in Table 1. Their high porosity and hydrophobicity are suitable features for MD operation, and the permeate fluxes achieved with these membranes are higher than those of polyvinylidene fluoride (PVDF) and polypropylene (PP) membranes in the AGMD configuration [19]. The entire module was held together with a set of bolts that ensured uniform compression of the gaskets and leak-free operation. Figure 1 illustrates the configuration of the membrane-based desorber.

Table 1. Specifications of the PTFE membranes used in this study.

Membrane ID	FGLP29325	FHLP29325
Nominal pore size (μm)	0.22	0.45
Porosity (%)	63	85
Thickness (μm)	128	175

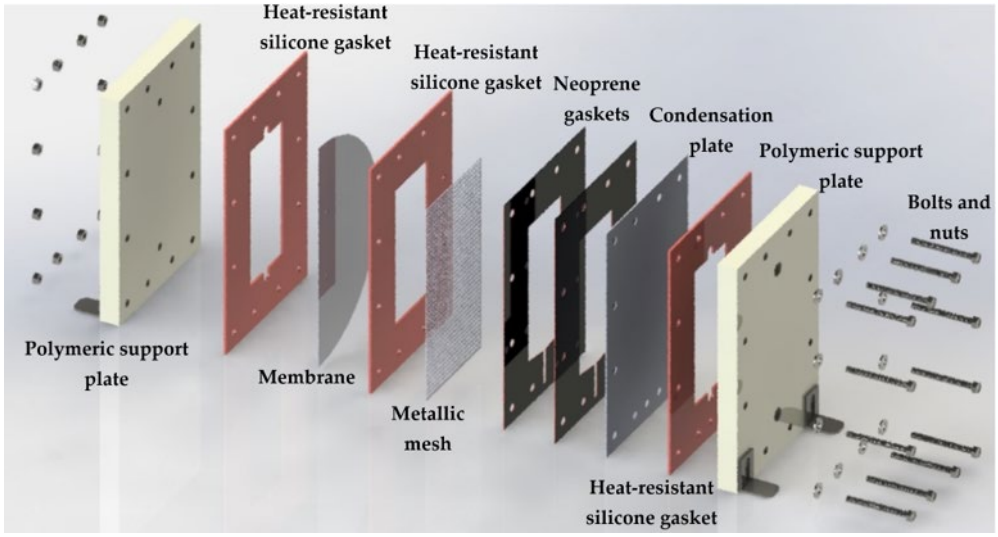


Figure 1. Membrane-based desorber.

2.3. Experimental System and Instrumentation

The experimental system included the membrane-based desorber, temperature-control equipment for the heating and cooling circuits, and the instrumentation required to monitor the operating variables. Heat was delivered to the saline solution through a secondary fluid circulated by a temperature-controlled heating unit (Julabo, Seelbach, Germany) and a plate heat exchanger (Alfa Laval, Lund, Sweden). On the cooling side, refrigerated water was circulated using a temperature-controlled unit with an integrated pump (Julabo, Seelbach, Germany).

Saline solution mass flow was measured using a Coriolis flowmeter (Emerson Electric Co., St. Louis, MO, USA), whereas analog flowmeters (Cole Parmer, Vernon Hills, IL, USA) were used for the heating fluid and cooling water. Gear pumps (Cole Parmer, Vernon Hills, IL, USA) provided circulation of the saline solution and heating fluid. The distilled water produced during each experiment was collected in previously weighed open containers. After collection, each container was weighed using an electronic balance

(Optima Scale, Rancho Cucamonga, CA, USA), and the mass of distilled water was determined from the difference between the final and initial container masses. Temperatures at the inlet and outlet of the membrane device and heat exchanger were measured using resistance temperature detector (RTD) Pt100 sensors (Omega Engineering, Stamford, CT, USA) and registered by a data acquisition unit (Agilent Technologies, Santa Clara, CA, USA).

The LiBr + LiCl/H_2O working solution was prepared from an aqueous LiBr solution (54% w/w, density of 1.57 kg/L at 25 °C) and crystalline LiCl powder, both supplied by Sigma-Aldrich (Burlington, MA, USA). The quantities of LiBr solution and LiCl were selected according to the desired initial salt concentration, while the final concentration was determined using the correlation reported in [13]. Figure 2 shows the experimental setup. Figure 3 illustrates the experimental system and its main components. The measurement uncertainties of the instruments are summarized in Table 2.

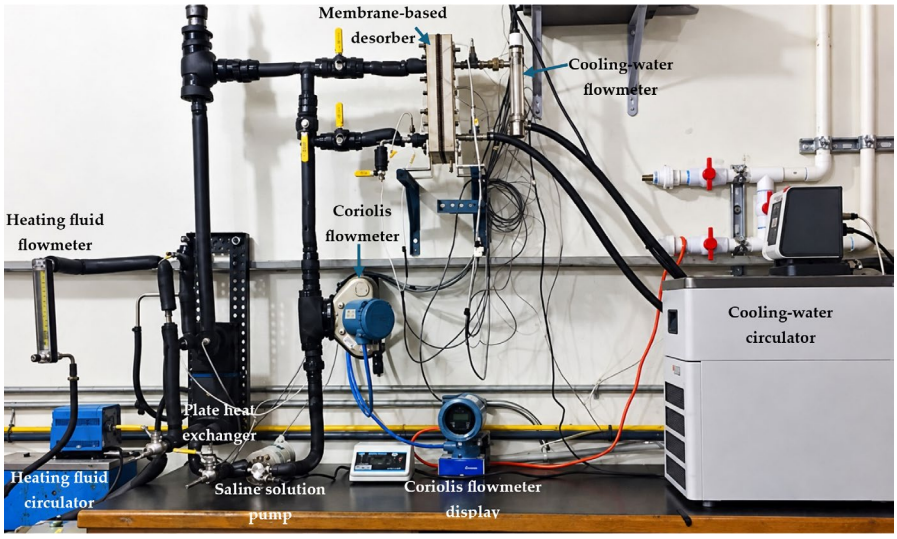


Figure 2. Experimental setup.

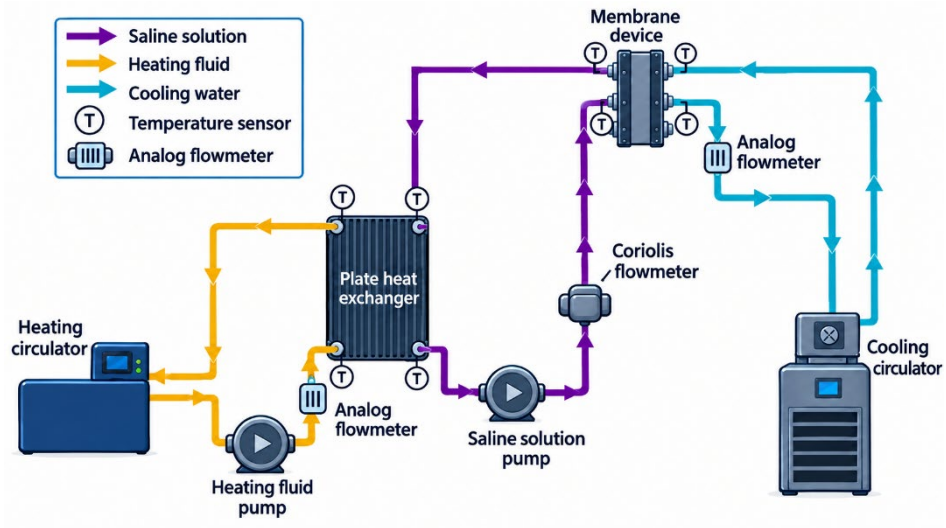


Figure 3. Schematic representation of the experimental system and its main components.

Table 2. Measurement ranges and uncertainties of the experimental instrumentation.

Variable	Sensor/Instrument	Measurement Range	Measurement Uncertainty
Temperature	RTD PT100	−30 to 350 °C	±0.1 °C
Cooling water volumetric flow	Volumetric flowmeter	0 to 8 L/min	±5.0% f.s. *
Heating fluid volumetric flow	Volumetric flowmeter	0 to 1.2 L/min	±4.0% f.s. *
Saline solution mass flow	Coriolis mass flowmeter	0 to 4.0×10^{-2} kg/s	±0.1%
Distilled water weight	Electronic balance	0 to 600 g	±0.01 g
Saline solution density	Coriolis mass flowmeter	0 to 5000 kg/m^3	±0.5 kg/m^3

* f.s., full scale.

2.4. Experimental Conditions

The membrane-based desorber was evaluated under different combinations of initial salt concentration and membrane pore size, as summarized in Table 3. A solution temperature of 90 °C was selected considering the thermal energy available from solar heating technologies. Previous experimental studies on solar-assisted LiBr/H_2O absorption chillers have reported hot-water temperatures close to 90 °C using evacuated-tube and flat-plate collectors, while the 80–90 °C range has also been identified as suitable for single-effect LiBr/H_2O absorption chillers coupled to solar collectors [20–22]. Therefore, 90 °C was considered an appropriate operating temperature for the membrane-based desorber when coupled to solar thermal or other low-grade heat sources [23,24]. Increasing the solution temperature also favors distilled water production by increasing the vapor-pressure driving force for mass transfer and decreasing solution viscosity [25]. Although membrane distillation can operate at temperatures below 90 °C, the desorption performance of concentrated absorbent solutions depends on the vapor-pressure difference between the feed solution and the condensation surface. Lower solution temperatures reduce this driving force and, consequently, distilled water production. In practical applications, the membrane-based desorber could be supplied with thermal energy from solar collectors or waste-heat recovery systems through a heat exchanger. However, the integration of these heat sources would require considering their thermal availability, operating temperature, the heating requirements of the desorption process, and the desired cooling capacity of the absorption cycle.

The condensation temperature was set at 30 °C to represent operating conditions compatible with air-cooled condensation under moderate ambient temperatures. This condition was considered to represent a system in which heat rejection could be achieved without a dedicated cooling-water circuit or cooling tower [26]. Previous experimental studies have demonstrated the feasibility of air-cooled membrane distillation configurations as an approach to simplify system design and reduce cooling-water requirements [27,28].

Table 3. Experimental conditions evaluated in this study.

Parameter	Value
Membrane pore size (μm)	0.22
	0.45
Initial salt concentration (% *w*/*w*)	50.01 ± 0.06
	44.96 ± 0.01
Cooling water mass flow (kg/s)	$(3.98 \pm 0.66) \times 10^{-2}$
Feed solution mass flow (kg/s)	$4.00 \times 10^{-2} \pm 6.87 \times 10^{-5}$
Feed solution temperature (°C)	90.2 ± 0.1
Cooling water temperature (°C)	30.0 ± 0.1

The amount of distilled water produced was collected and weighed at 30 min intervals throughout each experiment. All operating conditions were tested in duplicate, and the reported values correspond to the two independent runs.

3. Results

The performance of the membrane desorber operating with the LiBr + LiCl/H_2O mixture is discussed in terms of distilled water production, salt concentration increment, and comparison with two widely used aqueous working mixtures in absorption cooling systems.

3.1. Distilled Water Production Performance

Figure 4 presents the distilled water production obtained with the 0.22 and 0.45 µm membranes at initial salt concentrations of 50.01 and 44.96% *w*/*w* under the operating temperatures reported in Table 3. For all the evaluated conditions, distilled water production gradually declined as the experiment progressed. This trend is associated with the progressive increase in salt concentration in the feed solution caused by water removal. Consequently, the decrease in water activity leads to a reduction in the partial vapor pressure of water, thereby reducing the vapor-pressure driving force across the membrane [29]. Distilled water production was also higher with the 0.45 µm membrane. Previous AGMD studies have similarly reported that increasing membrane pore size favors permeate flux by reducing the resistance to vapor transport [30,31]. However, the effect of pore size became less pronounced at the higher salt concentration. At 50.01% *w*/*w*, the average distilled water production measured with the 0.45 µm membrane was only 4.8% higher than that measured with the 0.22 µm membrane. At the lowest salt concentration (44.96% *w*/*w*), the average distilled water production was 16.0% higher with the 0.45 µm membrane than with the 0.22 µm membrane. This behavior can be attributed to the reduced vapor-pressure driving force at higher salt concentrations, which limits the influence of membrane pore size on distilled water production. The influence of salinity on permeate production is also consistent with previous AGMD studies using highly saline solutions, in which permeate flux decreased with increasing salt concentration [32,33].

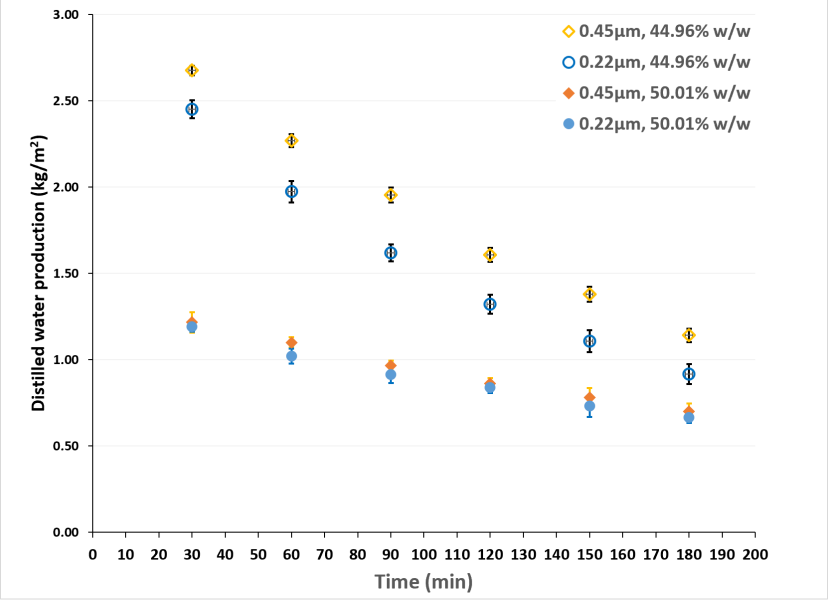


Figure 4. Distilled water production.

Figure 5 compares the cumulative distilled water production for the different initial salt concentrations and membrane pore sizes. It was 5.36 and 5.62 kg/m² at the highest salt concentration for the 0.22 and 0.45 µm membranes, respectively, whereas at the lowest salt concentration, the corresponding values increased to 9.39 and 11.03 kg/m², respectively, confirming the negative effect of increasing feed salinity on water production.

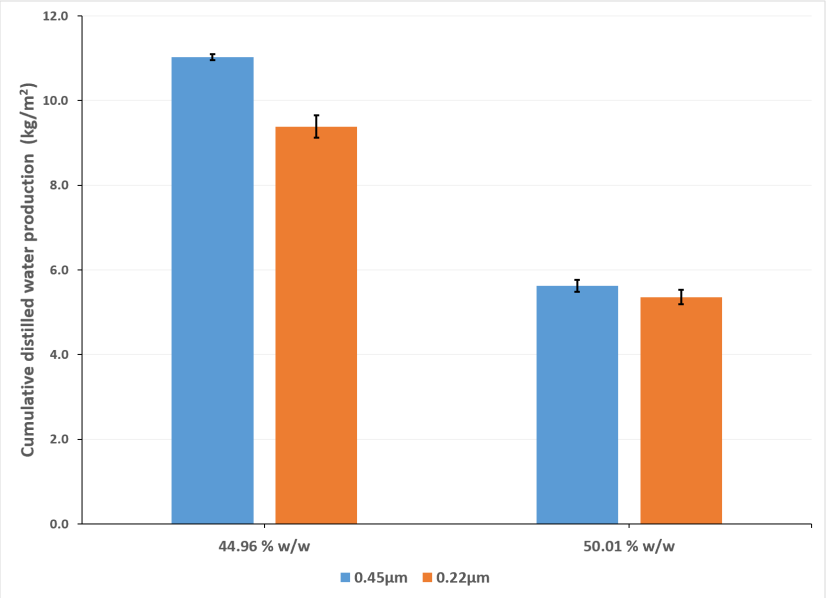


Figure 5. Cumulative distilled water production.

3.2. Concentration Increment

Figure 6 shows the evolution of salt concentration over time for the membrane pore sizes reported in Table 3. Consistent with the results presented in Section 3.1, the influence of membrane pore size on salt concentration was less pronounced at the higher initial salt concentration (50.01% *w*/*w*). Under this condition, the average salt concentration increment with the 0.45 µm membrane was 0.55% higher than that with the 0.22 µm membrane.

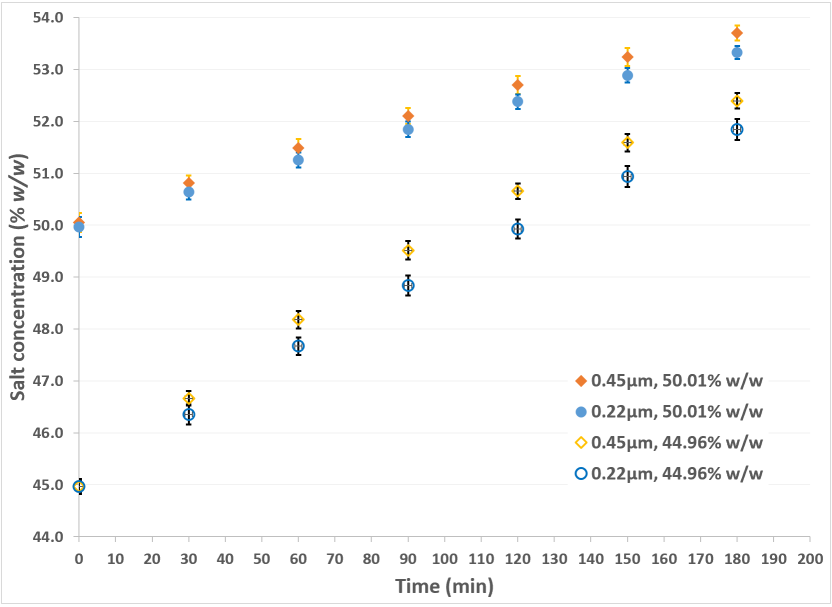


Figure 6. Salt concentration increment.

At the lowest initial salt concentration (44.96% *w*/*w*), this relative difference increased to 1.16%. The salt concentration increased from 50.01% *w*/*w* to 53.33% and 53.70% *w*/*w* with the 0.22 and 0.45 μm membranes, respectively. At the initial salt concentration of 44.96% *w*/*w*, the final concentrations were 51.85% and 52.40% *w*/*w* for the 0.22 and 0.45 μm membranes, respectively.

3.3. Comparison of Performance with LiBr/H₂O and LiCl/H₂O Mixtures

LiBr/H₂O is widely used in absorption cooling systems [34,35], while LiCl/H₂O has been investigated as an alternative working pair [36–38]. Both solutions provide relevant references for evaluating the performance of the LiBr + LiCl/H₂O mixture. Table 4 summarizes the experimental operating conditions reported for membrane desorbers using these working solutions and those employed in the present study.

Table 4. Experimental operating conditions reported in the literature and the present study.

Parameter	LiBr/H₂O [7]	LiCl/H₂O [39]	LiBr + LiCl/H₂O
Membrane pore size (μm)	0.45	0.22	0.22 0.45
Initial salt concentration (% *w*/*w*)	49.59 ± 0.10	40.98 ± 0.03	50.01 ± 0.06 44.96 ± 0.01
Cooling water mass flow (kg/s)	$(3.33 \pm 0.33) \times 10^{-2}$	$(3.32 \pm 0.58) \times 10^{-2}$	$(3.98 \pm 0.66) \times 10^{-2}$
Feed solution mass flow (kg/s)	$1.96\times 10^{-2} \pm 6.94 \times 10^{-4}$	$3.00 \times 10^{-2} \pm 4.90 \times 10^{-5}$	$4.00 \times 10^{-2} \pm 6.87 \times 10^{-5}$
Feed solution temperature (°C)	85.2 ± 0.5	90.3 ± 0.1	90.2 ± 0.1
Cooling water temperature (°C)	16.9 ± 0.5	30.1 ± 0.1	30.0 ± 0.1

Figure 7 compares the distilled water production of the LiBr/H₂O, LiCl/H₂O, and LiBr + LiCl/H₂O (2:1 mass ratio) mixtures under the operating conditions described in Table 4. As can be seen, the average distilled water production of the LiBr/H₂O mixture, evaluated using a membrane pore size of 0.45 μm and an initial salt concentration of 49.59% *w*/*w*, was 70.1% higher than that of the LiBr + LiCl/H₂O mixture, evaluated using a membrane pore size of 0.45 μm and an initial salt concentration of 50.01% *w*/*w*. This difference can be partially attributed to the fact that, although the initial salt concentration, membrane pore size, and feed solution temperature were similar, the cooling water temperature used with the LiBr/H₂O mixture was lower than that used with the LiBr + LiCl/H₂O mixture. This condition increases the vapor-pressure difference between the two sides of the membrane and enhances distilled water production. Although the solution mass flow rate was lower for the LiBr/H₂O mixture than for the LiBr + LiCl/H₂O mixture, its effect is less significant than that of an increase in the temperature difference [40,41]. However, when the LiBr + LiCl/H₂O mixture was operated with a 0.45 μm membrane and an initial salt concentration of 44.96% *w*/*w*, its distilled water production was up to 31.2% higher than that of the LiBr/H₂O mixture. The distilled water production of the LiBr + LiCl/H₂O mixture remained higher than that of the LiBr/H₂O mixture throughout the first 150 min of operation. At the final operating time (180 min), however, the distilled water production of the LiBr + LiCl/H₂O mixture was 5.3% lower than that of the LiBr/H₂O mixture.

For the experiments with the 0.22 μm membrane, the LiBr + LiCl/H₂O mixture at an initial salt concentration of 44.96% *w*/*w* showed higher distilled water production than LiCl/H₂O at 40.98% *w*/*w* during the first 120 min. The largest difference was observed at 30 min, when distilled water production with LiBr + LiCl/H₂O was 51.8% higher than that with LiCl/H₂O. Thereafter, the production difference gradually decreased, and the final distilled water production was 8.2% lower for the LiBr + LiCl/H₂O mixture than for the LiCl/H₂O mixture. The more pronounced decrease in distilled water production for the LiBr + LiCl/H₂O mixture may be associated with its higher initial salt concentration

(44.96% w/w) compared with LiCl/H_2O (40.98% *w*/*w*). As water was removed during operation, the resulting increase in salt concentration reduced the vapor-pressure driving force across the membrane, contributing to the lower distilled water production observed at the end of the experiment.

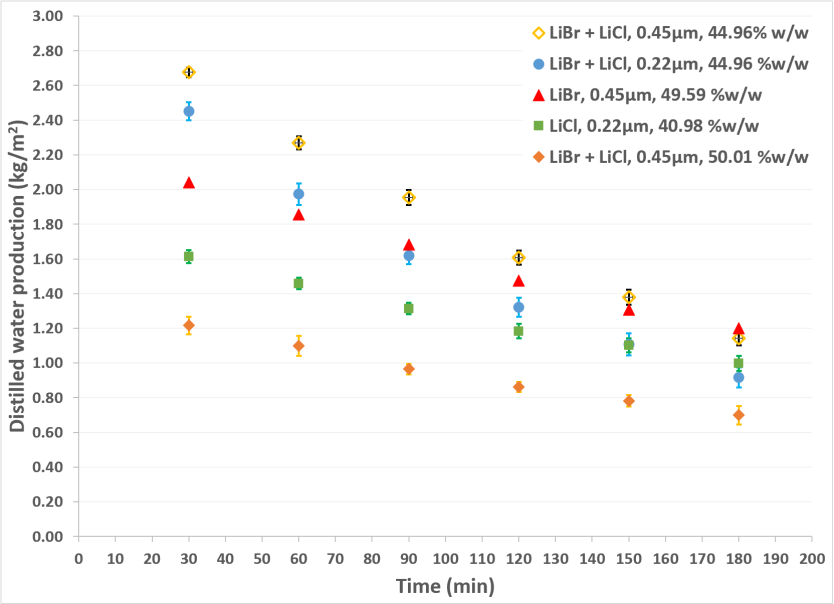


Figure 7. Comparison of distilled water production.

Figure 8 shows a comparison of the cumulative distilled water production of the analyzed mixtures. Under the operating conditions reported in Table 4, the cumulative distilled water production of the LiBr/H_2O mixture was 69.9% higher than that of the LiBr + LiCl/H_2O mixture. However, the cumulative distilled water production with the LiBr + LiCl/H_2O mixture, using a 0.22 µm membrane and an initial salt concentration of 44.96% *w*/*w*, was only 1.8% lower than that of the LiBr/H_2O mixture, demonstrating the potential of the LiBr + LiCl/H_2O mixture as a competitive alternative to LiBr/H_2O under the tested conditions. Despite the decrease in distilled water production observed over the course of the experiment in Figure 7, the cumulative production of the LiBr + LiCl/H_2O mixture was 22.4% higher than that of the LiCl/H_2O mixture.

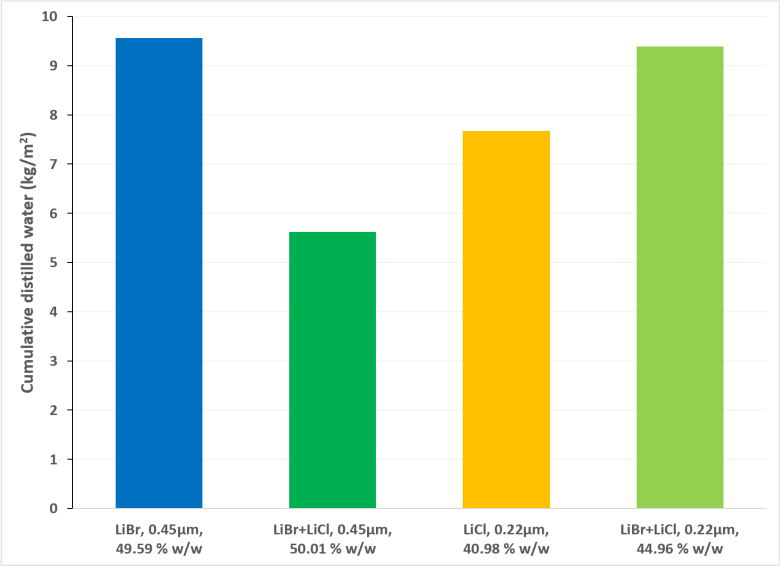


Figure 8. Comparison of cumulative distilled water production.

It should be noted that the comparisons presented in Figures 7 and 8 are based on experimental results obtained under different operating conditions, particularly regarding feed solution temperature, cooling-water temperature, and feed mass flow rate. As previously discussed, these parameters influence heat and mass transfer and the vapor-pressure driving force across the membrane. Therefore, the differences in distilled water production cannot be attributed exclusively to differences in the working solutions. Nevertheless, these comparisons provide a useful experimental reference for assessing the performance of the LiBr + LiCl/H_2O mixture relative to conventional working solutions under the reported operating conditions.

According to Chen and Xu [42], the higher membrane distillation performance of the LiBr/H_2O solution compared with LiCl/H_2O is associated with the higher diffusion coefficient of water molecules and more favorable interactions with the polymeric membrane. Although the LiCl/H_2O solution contained a greater number of free water molecules, the stronger interactions between Cl^- ions and the membrane, together with enhanced hydrogen bonding among water molecules, restricted water mobility. In contrast, LiBr/H_2O exhibited the highest water diffusion coefficient in the presence of the membrane, facilitating water transport and resulting in the highest transmembrane flux among the evaluated solutions. In a related study on interfacial evaporation, Guo et al. [43] reported that weaker interactions between water molecules and the evaporation surface can facilitate molecular detachment, thereby promoting faster evaporation. Additionally, Ren et al. [44] demonstrated that improving liquid distribution over the evaporation surface can enhance vapor transport and increase evaporation rates. These studies highlight the importance of interfacial interactions and mass transfer conditions in evaporation processes. Such phenomena are relevant to various water separation and treatment technologies, including membrane distillation [45] and solar-driven interfacial evaporation [46–48].

Overall, the LiBr + LiCl/H_2O mixture represents a promising working pair for intermittent absorption cooling systems, as it provided higher cumulative distilled water production than LiCl/H_2O under the evaluated conditions. Nevertheless, its thermophysical properties have not yet been comprehensively reported, making a complete comparison with conventional working pairs difficult. Recent studies have addressed the measurement of physical variables and the determination or prediction of thermophysical properties through advanced sensing technologies, experimental measurements, empirical correlations, thermodynamic models, and machine learning techniques [49–52]. However, further experimental measurements and thermodynamic modeling are required to determine the vapor pressure and other relevant properties of the LiBr + LiCl/H_2O mixture over a wider range of temperatures and salt concentrations for absorption cooling applications.

4. Conclusions

The performance of a membrane desorber with an AGMD configuration was evaluated using the LiBr + LiCl/H_2O mixture at a mass ratio of 2:1 (LiBr:LiCl). At the end of the 3 h experiment, cumulative distilled water production reached a maximum of 11.03 kg/m^2 at an initial salt concentration of 44.96% *w*/*w* with the 0.45 μm membrane, while the lowest value was 5.36 kg/m^2 at 50.01% *w*/*w* with the 0.22 μm membrane. The results showed that increasing the membrane pore size enhanced distilled water production, although the magnitude of this effect depended on the feed salinity. At 50.01% *w*/*w*, the average production with the 0.45 μm membrane was only 4.8% higher than that with the 0.22 μm membrane, whereas the difference increased to 16.0% at 44.96% *w*/*w*. The salt concentration increased from 50.01% *w*/*w* to 53.33% and 53.70% *w*/*w* with the 0.22 and 0.45 μm membranes, respectively, while at an initial concentration of 44.96% *w*/*w*, the final concentrations were 51.85% and 52.40% *w*/*w*, respectively. The performance comparison with LiBr/H_2O and LiCl/H_2O showed that, for the evaluated conditions, the average distilled

water production with LiBr/H_2O was 70.1% higher than that with the LiBr + LiCl/H_2O mixture. However, when the LiBr + LiCl/H_2O mixture was operated with a 0.45 μm membrane and an initial salt concentration of 44.96% *w*/*w*, its distilled water production was up to 31.2% higher than that of LiBr/H_2O and remained higher during the first 150 min of operation. At 180 min, its production was 5.3% lower than that of LiBr/H_2O. In contrast, under similar operating conditions, the LiBr + LiCl/H_2O mixture exhibited higher distilled water production than LiCl/H_2O during the first 2 h of operation, reaching a 51.8% higher production at 30 min. In terms of cumulative production, LiBr/H_2O produced 69.9% more distilled water than LiBr + LiCl/H_2O, whereas the latter produced 22.4% more than LiCl/H_2O. However, with a 0.22 μm membrane and an initial salt concentration of 44.96% *w*/*w*, the cumulative distilled water production with the LiBr + LiCl/H_2O mixture was only 1.8% lower than that obtained with LiBr/H_2O. Moreover, with the 0.45 μm membrane and an initial salt concentration of 44.96% *w*/*w*, LiBr + LiCl/H_2O reached its highest cumulative distilled water production, which was 15.4% higher than the value for LiBr/H_2O.

The present study was limited to a single feed solution temperature and cooling-water temperature, and the comparisons with LiBr/H_2O and LiCl/H_2O were based on experimental results obtained under different operating conditions. In addition, the thermophysical properties of the LiBr + LiCl/H_2O mixture have not yet been comprehensively characterized. Although the operating temperature of the membrane-based desorber is compatible with temperatures achievable using suitable solar thermal systems, its integration with practical heat sources has not yet been experimentally evaluated. Overall, the competitive distilled water production achieved with the LiBr + LiCl/H_2O mixture in the present study supports its potential as an alternative working solution for membrane-based intermittent absorption cooling systems.

Author Contributions: Conceptualization, J.I.-B., U.D.-C., Y.R.G.-L., A.L.-J., and W.R.; methodology, J.I.-B., U.D.-C., Y.R.G.-L., A.L.-J., and W.R.; formal analysis, J.I.-B., U.D.-C., Y.R.G.-L., A.L.-J., and W.R.; writing—original draft preparation, J.I.-B., U.D.-C., Y.R.G.-L., A.L.-J., and W.R.; writing—review and editing, J.I.-B., U.D.-C., Y.R.G.-L., A.L.-J., and W.R.; supervision, J.I.-B., U.D.-C., Y.R.G.-L., A.L.-J., and W.R.; project administration, W.R.; funding acquisition, W.R. All authors have read and agreed to the published version of the manuscript.

Funding: This research was funded by the UNAM-PAPIIT-IT102224 project.

Data Availability Statement: The original contributions presented in this study are included in the article. Further inquiries can be directed to the corresponding author.

Acknowledgments: The authors gratefully acknowledge the support of the UNAM-PAPIIT project IT102224. Arelis Ledesma Juárez acknowledges the postdoctoral fellowship granted by SECIHTI through the program "Estancias Posdoctorales por México". Ulises Dehesa-Carrasco acknowledges the postdoctoral fellowship granted by SECIHTI through the program "Estancias Posdoctorales para Personas Indígenas". Jonathan Ibarra-Bahena acknowledges the postdoctoral fellowship granted by SECIHTI through the program "Estancias Posdoctorales por México para la Formación y Consolidación de las y los Investigadores por México". During the preparation of this manuscript, the authors used (GPT-6, OpenAI, San Francisco, CA, USA) to improve the visual presentation of Figure 3 based on the original schematic provided by the authors. The authors have reviewed and edited the output and take full responsibility for the content of this publication.

Conflicts of Interest: The authors declare no conflicts of interest.

References

1. Vautrin, A.; Dou, J.; Nordin Furdos, A.; Voswinkel, F. Cooling a Hotter World: El Niño Meets Strong Growth in Global Electricity Demand. *International Energy Agency (IEA)*, Commentary, 10 July 2026. Available online: https://www.iea.org/commentaries/cooling-a-hotter-world-el-nino-meets-strong-growth-in-global-electricity-demand (accessed on 4 August 2026).
2. Brown, J.S.; Domanski, P.A. Review of Alternative Cooling Technologies. *Appl. Therm. Eng.* **2014**, *64*, 252–262.
3. Srikhirin, P.; Aphornratana, S.; Chungpaibulpatana, S. A review of absorption refrigeration technologies. *Renew. Sustain. Energy Rev.* **2001**, *5*, 343–372.
4. Wang, L.; He, L.; He, Y. Review on Absorption Refrigeration Technology and Its Potential in Energy-Saving and Carbon Emission Reduction in Natural Gas and Hydrogen Liquefaction. *Energies* **2024**, *17*, 3427.
5. Verma, A.; Chakraborty, P.R. Water–Lithium bromide absorption chillers for solar cooling. In *Solar Energy Conversion Systems*; Kalogirou, S.A., ed.; Springer: Singapore, 2018; pp. 209–232.
6. Nguyen, N.-H.; Hoang, Q.-A.; Le, H.-C.; Hoang, H.-D. Theoretical and Experimental Study of Intermittent Absorption Refrigeration System. In Proceedings of the 2018 4th International Conference on Green Technology and Sustainable Development (GTSD), Ho Chi Minh City, Vietnam, 23–24 November 2018; pp. 436–441.
7. Ibarra-Bahena, J.; Rivera, W.; Romero, R.J.; Montiel-González, M.; Dehesa-Carrasco, U. Novel intermittent absorption cooling system based on membrane separation process. *Appl. Therm. Eng.* **2018**, *136*, 718–729.
8. Ibrahim, A.G.M.; Dincer, I. Experimental performance evaluation of a combined solar system to produce cooling and potable water. *Sol. Energy* **2015**, *122*, 1066–1079.
9. Rivera, W.; Moreno-Quintanar, G.; Rivera, C.O.; Best, R.; Martínez, F. Evaluation of a solar intermittent refrigeration system for ice production operating with ammonia/lithium nitrate. *Sol. Energy* **2011**, *85*, 38–45.
10. Moreno-Quintanar, G.; Rivera, W.; Best, R. Comparison of the experimental evaluation of a solar intermittent refrigeration system for ice production operating with the mixtures $NH_3/LiNO_3$ and $NH_3/LiNO_3/H_2O$. *Renew. Energy* **2012**, *38*, 62–68.
11. Talpada, J.S.; Ramana, P.V. A review on performance of absorption refrigeration system using new working pairs and nanoparticles. *Int. J. Ambient Energy* **2022**, *43*, 5654–5672.
12. Papadopoulos, A.I.; Kyriakides, A.-S.; Seferlis, P.; Hassan, I. Absorption refrigeration processes with organic working fluid mixtures—A review. Renew. Sustain. *Energy Rev.* **2019**, *109*, 239–270.
13. Arabi, M.; Dehghani, M.R. Measurement of solubility and density of water + lithium bromide + lithium chloride and water +lithium bromide + sodium formate systems. *Int. J. Refrig.* **2015**, *56*, 99–104.
14. Aktemur, C.; Öztürk, İ.T. Energetic and exergetic analysis of a solar-driven single-effect absorption refrigeration system using LiBr+LiCl/H_2O solution mixture. *J. Sol. Energy Eng.* **2022**, *144*, 061007.
15. Aktemur, C.; Öztürk, İ.T. Thermodynamic optimization of utilization of LiBr+LiCl/H_2O solution mixture on a single-effect absorption chiller driven by solar energy. *J. Sol. Energy Eng.* **2023**, *145*, 051003.
16. Ibarra-Bahena, J.; Dehesa-Carrasco, U.; Galindo-Luna, Y.R.; Medina-Caballero, I.L.; Rivera, W. Membrane Separation for the Treatment of LiBr + LiCl Brines and Their Application. *Membranes* **2025**, *15*, 219.
17. Guillen-Burrieza, E.; Blanco, J.; Zaragoza, G.; Alarcón, D.-C.; Palenzuela, P.; Ibarra, M.; Gernjak, W. Experimental analysis of an air gap membrane distillation solar desalination pilot system. *J. Membr. Sci.* **2011**, *379*, 386–396.
18. Alkhudhiri, A.; Darwish, N.; Hilal, N. Produced water treatment: Application of Air Gap Membrane Distillation. *Desalination* **2013**, *309*, 46–51.
19. He, K.; Hwang, H.J.; Moon, I.S. Air gap membrane distillation on the different types of membrane. *Korean J. Chem. Eng.* **2011**, *28*, 770–777.
20. Syed, A.; Izquierdo, M.; Rodríguez, P.; Maidment, G.; Missenden, J.; Lecuona, A.; Tozer, R. A Novel Experimental Investigation of a Solar Cooling System in Madrid. *Int. J. Refrig.* **2005**, *28*, 859–871.
21. Chen, J.F.; Dai, Y.J.; Wang, R.Z. Experimental and Analytical Study on an Air-Cooled Single-Effect LiBr–H_2O Absorption Chiller Driven by Evacuated Glass Tube Solar Collector for Cooling Application in Residential Buildings. *Sol. Energy* **2017**, *151*, 110–118.
22. Wang, R.Z.; Xu, Z.Y.; Pan, Q.W.; Du, S.; Xia, Z.Z. Solar Driven Air Conditioning and Refrigeration Systems Corresponding to Various Heating Source Temperatures. *Appl. Energy* **2016**, *169*, 846–856.
23. Abu-Zeid, M.A.; Bassyouni, M.; Fouad, Y.; Monica, T.; Sandid, A.M.; Elhenawy, Y. Experimental and Simulation Study of Solar-Powered Air-Gap Membrane Distillation Technology for Water Desalination. *Membranes* **2023**, *13*, 821.
24. Yadav, A.; Labhasetwar, P.K.; Shahi, V.K. Membrane Distillation Using Low-Grade Energy for Desalination: A Review. *J. Environ. Chem. Eng.* **2021**, *9*, 105818.

https://doi.org/10.3390/membranes16120406

25. Schwantes, R.; Bauer, L.; Chavan, K.; Dücker, D.; Felsmann, C.; Pfafferott, J. Air Gap Membrane Distillation for Hypersaline Brine Concentration: Operational Analysis of a Full-Scale Module—New Strategies for Wetting Mitigation. *Desalination* **2018**, *444*, 13–25.
26. Xu, Z.; Wang, R. Comparison of absorption refrigeration cycles for efficient air-cooled solar cooling. *Sol. Energy* **2018**, *172*, 14–23.
27. Cong, S.; Miao, Q.; Guo, F. Mass Transfer Analysis of Air-Cooled Membrane Distillation Configuration for Desalination. *Membranes* **2021**, *11*, 281.
28. Narayan, A.; Pitchuman, R. Analysis of an air-cooled air gap membrane distillation module. *Desalination* **2020**, *475*, 114179.
29. Martínez, L. Comparison of membrane distillation performance using different feeds. *Desalination* **2004**, *168*, 359–365.
30. Izquierdo-Gil, M.A.; García-Payo, M.C.; Fernández-Pineda, C. Air gap membrane distillation of sucrose aqueous solutions. *J. Membr. Sci.* **1999**, *155*, 291–307.
31. Alkhudhiri, A.; Darwish, N.; Hilal, N. Treatment of saline solutions using Air Gap Membrane Distillation: Experimental study. *Desalination* **2013**, *323*, 2–7.
32. Alkhudhiri, A.; Darwish, N.; Hilal, N. Treatment of high salinity solutions: Application of air gap membrane distillation. *Desalination* **2012**, *287*, 55–60.
33. Alkhudhiri, A.; Hilal, N. Air gap membrane distillation: A detailed study of high saline solution. *Desalination* **2017**, *403*, 179–186.
34. Sun, J.; Fu, L.; Zhang, S. A review of working fluids of absorption cycles. *Renew. Sustain. Energy Rev.* **2012**, *16*, 1899–1906.
35. Wu, X.; Jing, T.; Han, S.; Wang, L.; Leng, Q.; Xu, S. Applicability, progress and prospect of water-based and ionic liquid-based working pairs in absorption refrigeration system. *Renew. Sustain. Energy Rev*. **2026**, *235*, 116985.
36. Bellos, E.; Tzivanidis, C.; Antonopoulos, K.A. Exergetic and energetic comparison of LiCl–H_2O and LiBr–H_2O working pairs in a solar absorption cooling system. *Energy Convers. Manag.* **2016**, *123*, 453–461.
37. Pandya, B.; Modi, N.; Upadhyai, R.; Patel, J. Thermodynamic performance and comparison of solar assisted double effect absorption cooling system with LiCl–H_2O and LiBr–H_2O working fluid. *Build. Simul.* **2019**, *12*, 1063–1075.
38. Bhowmick, A.; Kundu, B. Thermo-economic optimization and comparison study of LiBr-H_2O and LiCl-H_2O working pair in absorption cooling systems based on genetic algorithm. *Int. J. Energy Res.* **2021**, *45*, 3938–3954.
39. Ibarra-Bahena, J.; Dehesa-Carrasco, U.; Galindo-Luna, Y.R.; Medina-Caballero, I.L.; Rivera, W. Experimental Performance of a Membrane Desorber with a H_2O/LiCl Mixture for Absorption Chiller Applications. *Membranes* **2022**, *12*, 1184.
40. Kalla, S.; Upadhyaya, S.; Singh, K. Principles and Advancements of Air Gap Membrane Distillation. *Rev. Chem. Eng.* **2019**, *35*, 817–859.
41. Ibarra-Bahena, J.; Dehesa-Carrasco, U.; Romero, R.; Rivas-Herrera, B.; Rivera, W. Experimental assessment of a hydrophobic membrane-based desorber/condenser with H_2O/LiBr mixture for absorption systems. *Exp. Therm. Fluid Sci.* **2017**, *88*, 145–159.
42. Chen, Y.; Xu, X. Molecular Dynamics Study on the Influence of Working Pairs on Membrane Distillation Process Applied in Absorption Refrigeration Systems. *J. Mol. Liq.* **2025**, *433*, 127796.
43. Guo, S.; Yu, Z.; Tan, S.C. Boosting water evaporation with clever surface design. *Nat. Sustain.* **2026**. https://doi.org/10.1038/s41893-026-01843-6
44. Ren, J.; Xu, J.; Tian, S.; Shi, K.; Gu, T.; Zhao, J.; Li, X.; Zhou, Z.; Tijing, L.; Shon, H.K. Hydrodynamic solar-driven interfacial evaporation—Gone with the flow. *Water Res.* **2024**, *266*, 122432.
45. Chang, H.; Liu, B.; Zhang, Z.; Pawar, R.; Yan, Z.; Crittenden, J.C.; Vidic, R.D. A critical review of membrane wettability in membrane distillation from the perspective of interfacial interactions. *Environ. Sci. Technol.* **2021**, *55*, 1395–1418.
46. Tian, S.; Zhou, Z.; Li, X.; Wang, F.; Zhao, Y.; Tijing, L.; Shon, H.K.; Xu, B.; Ren, J. Applications of solar-driven interfacial evaporation-coupled photocatalysis in water treatment: A mini review. *Desalination* **2024**, *592*, 118159.
47. Zhou, M.; Zhang, L.; Tao, S.; Li, R.; Wang, Y. Recent research advances in efficient solar-driven interfacial evaporation. *Chem. Eng. J.* **2024**, *489*, 151157.
48. Srishti; Sinhamahapatra, A.; Kumar, A. Review of the progress of solar-driven interfacial water evaporation (SIWE) toward a practical approach. *Energy Adv.* **2023**, *2*, 574–605.
49. Wei, Y.; Hao, R.; Hong, X.; Guo, S.; Lu, D.; Li, H.; Zhao, W.; Tang, Z.; Zhou, C.; Cao, W.; et al. Intelligent Temperature and Pressure Sensing Decoupling Systems in Multimodal Nanonetwork-based Electronic Textiles. *ACS Nano* **2026**, *20*, 16216–16229.
50. Lv, X.; Li, M.; Yang, Y.; He, M.; Zhou, C.; Luo, C. Vapor Pressure, Density, Viscosity, Specific Heat Capacity, Dissolution Enthalpy, and Specific Enthalpy of the LiCl–[BMIM]Cl/H_2O Working Pair. *J. Chem. Eng. Data* **2026**, *71*, 1641–1649.

51. Schwaab, G.; Pezzotti, S. A New Perspective on Aqueous Electrolyte Solutions. *Phys. Chem. Chem. Phys.* **2025**, *27*, 17585–17597.
52. Zante, G. Machine Learning for Determination of Activity of Water and Activity Coefficients of Electrolytes in Binary Solutions. *Artif. Intell. Chem.* **2024**, *2*, 100069.

Disclaimer/Publisher's Note: The statements, opinions and data contained in all publications are solely those of the individual author(s) and contributor(s) and not of MDPI and/or the editor(s). MDPI and/or the editor(s) disclaim responsibility for any injury to people or property resulting from any ideas, methods, instructions or products referred to in the content.